Topics in Catalysis (2024) 67:910–921
https://doi.org/10.1007/s11244-024-01926-8

ORIGINAL PAPER

Tuning the Interaction Between Ru Nanoparticles and Nd_2O_3 to Enhance Hydrogen Formation from Ammonia Decomposition

Xiaohua Ju[1] · Lin Liu[1,2] · Teng He[1,2] · Ping Chen[1,2]

Accepted: 19 February 2024 / Published online: 28 March 2024

Abstract

Development of highly active and stable catalysts for production of CO_x-free hydrogen from ammonia is crucial for the use of ammonia as hydrogen carrier. Herein, Ru nanoparticles (NPs) on Nd_2O_3 (Ru/Nd_2O_3) was prepared by different methods and investigated for NH_3 decomposition reaction. The dependence of the catalytic activity of Ru NPs on the Nd_2O_3 on the interaction between Ru NPs and Nd_2O_3 support was investigated in detail. The Ru/Nd_2O_3 obtained from precipitation method exhibits a high hydrogen formation rate of 1548 mmol g_{cat}^{-1} h^{-1} at 450 °C, which is high than that of the Ru/Nd_2O_3 analogue from milling method and comparable with many efficient oxides supported Ru catalysts reported previously. As revealed by various characterization techniques, the high activity of Ru/Nd_2O_3 obtained from precipitation method can be attributed to the enhanced interaction between Ru NPs and Nd_2O_3. The Ru NPs in Ru/Nd_2O_3 analogue with enhanced the metal-support interaction can modulate electronic structure and facilitate the activation and decomposition of NH_3. Therefore, Ru/Nd_2O_3 obtained from precipitation method exhibited significantly improved activity and intrinsic activity for NH_3 decomposition. This study provides promise for the design of efficient Ru/Nd_2O_3 catalyst for NH_3 decomposition reaction by tuning the metal–support interaction of catalysts.

Keywords Ru nanoparticles · Nd_2O_3 · Catalyst · Ammonia decomposition · Metal–support interaction

1 Introduction

Hydrogen is one of the most promising energy carriers for the future energy systems, but the low volumetric energy density of hydrogen (in both compressed gas and liquid forms) makes the storage of hydrogen a difficult problem [1]. Ammonia has been considered as one of the most promising hydrogen carriers for the high gravimetric (17.7 wt% H_2) and volumetric (121 kg H_2 m^{-3} in the liquid form) H_2 density, high energy density, liquid state under mild conditions and billion tons of annual production in world-wide [2–4]. The decomposition of NH_3, a critical step for production of H_2 from NH_3, is thermodynamically favorable under relatively low-temperature conditions. However, the sluggish kinetics of NH_3 decomposition reaction greatly limits the production of H_2 from decomposition of NH_3. Thus, it is extremely expected to develop efficient catalysts exhibiting high catalytic activity and good stability for decomposition of NH_3 at relatively low temperature [3, 5].

Among the different kinds of NH_3 decomposition catalysts, supported Ru catalysts usually show high activity and stability for decomposition of NH_3 [6–9]. It is generally accepted that the catalytic performances of supported Ru catalysts in NH_3 decomposition are mainly determined by the active sites on the surface of Ru nanoparticles (NPs), which are closely correlated with the size, shape and interfacial structure between Ru NPs and oxide supports. As multicomponent catalyst systems, the catalytic performances of oxide supported Ru catalysts rely not only on the structure of Ru NPs but also on the properties of oxide supports. Usually, the catalytic performances of supported Ru catalysts in NH_3 decomposition is strongly related to the properties of the oxide supports [7, 8, 10–12]. Previous studies show

✉ Lin Liu
liulin@dicp.ac.cn

✉ Teng He
heteng@dicp.ac.cn

[1] Dalian National Laboratory for Clean Energy, Dalian Institute of Chemical Physics, Chinese Academy of Sciences, 457 Zhongshan Road, Dalian 116023, China

[2] Center of Materials Science and Optoelectronics Engineering, University of Chinese Academy of Sciences, Beijing 100049, China

that oxides such as SiO_2 [11, 13, 14], TiO_2 [8], zeolite [14], Al_2O_3 [15, 16], MgO [8, 17–19], ZrO_2 [20–22], La_2O_3 [23], barium hexaaluminate [24], Y_2O_3 [25], Pr_2O_3 [26] and Sm_2O_3 [27] are efficient supports for Ru-based catalysts.

Currently, development of new kind of oxide supported Ru catalysts is still highly desirable for expanding the scope of Ru-based NH_3 decomposition catalysts. In recent years, neodymium oxide (Nd_2O_3) has attracted much attention due to its properties such as high chemical stability and high thermal conductivity. Also, the Nd_2O_3 materials have been widely applied as catalysts or supports in catalysis [28–32]. Nd_2O_3 is a promising support for the metal-based catalysts due to its ability to stabilize the active metal phase with high dispersion. Currently, Nd_2O_3 supported Co catalysts have been investigated in ammonia synthesis reaction [31, 32]. It has long been known that the function of oxide support is not only to disperse and stabilize metal particles but also to generate interface phenomena through metal–oxide interaction. Recently, the role of metal–support interaction in tuning the electronic properties and catalytic performances of oxide (e.g., FeO_x, CeO_2 and TiO_2) supported metal NPs has been recognized in different catalytic reactions [33, 34]. However, little attention has been paid to the use of Nd_2O_3 for construction of efficient Nd_2O_3 supported Ru NPs catalyst with excellent activity and stability for NH_3 decomposition. Meanwhile, the importance of the metal–support interaction in modulating the catalytic performances of Nd_2O_3 supported Ru catalysts in NH_3 decomposition has not been recognized up to now.

Here, Ru/Nd_2O_3 analogues consisting of nearly identical Ru NPs and Nd_2O_3 by different methods (milling and precipitation method) were prepared and evaluated as catalysts for NH_3 decomposition reaction. Compared with Ru/Nd_2O_3 obtained from milling method, Ru/Nd_2O_3 obtained from precipitation method has remarkably improved activity for NH_3 decomposition under identical reaction conditions. A variety of characterization techniques have been applied to study the relationship between the catalytic performance and the structure of Ru/Nd_2O_3 catalysts obtained from different methods in detail, which reveal that the catalytic activity of Ru/Nd_2O_3 catalysts show high dependence on the interaction between the Ru NPs and Nd_2O_3 support.

2 Experimental

2.1 Preparation of Ru/Nd_2O_3 Catalysts

The support precursor of $Nd(OH)_3$ was prepared by modifying established method [35]. First, $Nd(NO_3)_3{\cdot}6H_2O$ and KOH were dissolved in deionized water (0.5 M), respectively. Then the $Nd(NO_3)_3$ solution was added into the KOH solution under stirring for 10 min. The mixture was transferred into a Teflon-lined stainless autoclave at 180 °C for 12 h. The $Nd(OH)_3$ was obtained via filtration, washing and drying at 80 °C for 12 h.

The Ru/Nd_2O_3-p samples with Ru mass loading of 1.5 wt% and 3 wt% were synthesized by precipitation method. Typically, 0.36 g of $Nd(OH)_3$ and 0.09 g of KOH were dispersed in 30 mL of water. Subsequently, a designated amount of $RuCl_3$ solution (0.007 M) was slowly added under vigorous stirring [36]. The mixture was stirred 2 h at room temperature. The solid was obtained by filtration, and then washed with deionized water. Finally, the product was dried at 80 °C for 12 h. The Ru/Nd_2O_3-p samples were obtained by reduction in 10% H_2/N_2 atmosphere at 500 °C for 2 h.

For comparison, 1.5 wt% and 3 wt% Ru/Nd_2O_3-m samples were prepared using milling method from $Nd(OH)_3$ and RuO_2 NPs. The preparation of RuO_2 NPs is similar to the precipitation method for preparing Ru/Nd_2O_3-p catalyst. A designated amount of $RuCl_3$ solution (0.007 M) was slowly added to the KOH solution (0.12 M) under vigorous stirring. The mixture was stirred 2 h at room temperature. The RuO_2 NPs was obtained by filtration. In a typical synthesis, desired amount of $Nd(OH)_3$ and RuO_2 NPs were ground in a mortar for 20 min. The Ru/Nd_2O_3-m samples were obtained by reduction in 10% H_2/N_2 atmosphere at 500 °C for 2 h.

2.2 Characterization

X-ray diffraction (XRD) measurements were performed with Cu Kα radiation using an X'Pert Pro (PANAlytical) diffractometer.

The specific surface area of the catalysts was obtained by means of a nitrogen adsorption–desorption isotherm collected at − 196 °C using a Micromeritics ASAP 2020 analyzer. The samples were heated to 300 °C in a flow of N_2 for 8 h prior to the experiment. The specific surface area was calculated by the Brunauer–Emmet–Teller (BET) method at the N_2 relative pressure range of $0.05 < P/P_0 < 0.30$.

To determine the morphology and size of the catalysts, transmission electron microscopy (TEM) measurements were performed on a JEOL 2100X. The samples were prepared by ultrasonic dispersion of powders in ethanol and a droplet of the dispersion was then placed onto a copper grid. The dispersion of Ru particles (D_{Ru}) was calculated using the equation by Borodziński and Bonarowska [36]:

$$D_{Ru} = \sqrt[1.23]{\frac{d_{at} \times 3.32}{d_{TEM}}} \quad \text{for } 0.2 \le D_{Ru} \le 0.92.$$

$$D_{Ru} = \frac{d_{at} \times 5.01}{d_{TEM}} \quad \text{for} D_{Ru} < 0.2.$$

where d_{at} is the atomic diameter of Ru (0.269 nm).

The exposed Ru dispersion of the catalyst was measured by CO pulse chemisorption using an AutoChem 2910. About 100 mg of the catalyst was reduced at 400 °C for 1 h in 10% H_2/Ar (30 mL min^{-1}) prior to the pulse CO chemisorption measurement, and then cooled down to room temperature in He (30 mL min^{-1}). The CO uptake was measured using a gas chromatograph equipped with a TCD detector. The Ru dispersion was calculated by assuming a CO:Ru stoichiometry of 1:1.

Temperature programmed reduction (TPR) was performed with a fixed-bed reactor equipped with a gas chromatograph. TPR experiments were carried out from 30 to 800 °C (10 °C min^{-1}) under 5% H_2/Ar with a flow rate of 30 mL min^{-1}.

CO adsorption diffuse reflectance infrared Fourier transform spectroscopy (DRIFTS) studies were performed to monitor the gas–solid interface using a Bruker TENSOR II equipped with a mercury cadmium telluride detector and operated at a resolution of 4 cm^{-1} for 16 scans. Previous to the CO adsorption experiment, the IR cell with catalyst was purged in Ar at room temperature for 0.5 h, and the spectrum was recorded as the background. Then a 5% CO/Ar mixture flow was switched to the IR cell for 0.5 h. Afterward, the chamber was purged with Ar (30 mL min^{-1}) for 0.5 h to remove gaseous CO before the spectrum featuring CO adsorption was recorded.

X-ray photoelectron spectroscopy (XPS) measurement was performed on an ESCALAB MK-II spectrometer with Al Ka as the excitation source. Carbonaceous C 1s line (284.8 eV) was used as the reference to calibrate the binding energy.

2.3 Catalytic Reaction Test

Catalytic tests were carried out on a continuous fixed-bed flow quartz reactor. The dried catalysts (20–40 mesh) were reduced in an 10% H_2/Ar (30 mL min^{-1}) flow at 500 °C for 2 h. Then pure NH_3 was inputted with a flow rate of 25 mL min^{-1}. All the activity tests of catalysts were conducted under atmospheric pressure, and pure NH_3 was used as the only reactant. The reaction temperature was in the range of 300–550 °C. The activity tests of catalysts with different weight hourly space velocity (WHSV) values in NH_3 stream were conducted at 450 °C. Product gas composition was analyzed by on-line gas chromatograph (GC-7890A, Agilent) equipped with a thermal conductivity detector and Porapak N column. The tested reaction temperature was in the range of 300–500 °C.

3 Results and Discussion

3.1 Structure Characterization of Catalysts

In this study, RuO_2 NPs were firstly synthesized using precipitation method. Figure S1 shows TEM images of RuO_2 NPs in different scale. It is obvious that RuO_2 colloid NPs have a spherical-like morphology with a uniform particle size with an average particle size of 1.9 ± 0.2 nm (Fig. S1). Well-crystallized Nd_2O_3 were used as the support precursor to disperse RuO_2 NPs. Precipitation and solid milling were applied to disperse highly dispersed RuO_2 NPs onto the Nd_2O_3 support (Scheme 1). The samples were reduced at 500 °C, and the obtained Ru/Nd_2O_3 catalysts were denoted as 1.5% Ru/Nd_2O_3-m, 3% Ru/Nd_2O_3-m, 1.5% Ru/Nd_2O_3-p and 3% Ru/Nd_2O_3-p samples, respectively.

To investigate the structure of the catalysts, the XRD patterns of Ru/Nd_2O_3 samples obtained from different methods and Nd_2O_3 support are shown in Fig. 1. Similar with that of the Nd_2O_3 (JCPDS 00-121-0579), it was seen from the pattern that the diffraction peaks of Nd_2O_3 support were relatively wide, which was related to the low degree of crystallinity of the support. After loading of Ru NPs on the Nd_2O_3 support, no characteristic diffraction peak of Ru (JCPDS 011253) can be found in the XRD patterns of Ru/Nd_2O_3 samples obtained from different methods. This is related to the high dispersion of Ru NPs on the support surface. The major characteristic peak intensity of Ru/Nd_2O_3-m samples was similar with that of the Nd_2O_3 support, indicating the well preservation of Nd_2O_3 in Ru/Nd_2O_3-m samples. By contrast, the diffraction peak intensity of the 1.5% Ru/Nd_2O_3-p and 3% Ru/Nd_2O_3-p catalysts were much stronger than that of the Nd_2O_3 support, which indicates that the crystallinity of the Nd_2O_3 in the Ru/Nd_2O_3-p catalysts was improved.

Table S1 shows the specific surface area and average Ru particle size (estimated by TEM) of the Ru/Nd_2O_3 catalysts. The BET surface areas of Ru/Nd_2O_3 samples and Nd_2O_3 support are summarized in Table S1. The Nd_2O_3 support has a high surface area of 70.6 m^2 g^{-1}. It is obvious that the BET surface areas of Ru/Nd_2O_3-m samples decrease obviously after the deposition of Ru NPs. In comparison with that of the Ru/Nd_2O_3-m samples, Ru/Nd_2O_3-p samples possess relatively large surface areas. The influence of preparation method on the particle size of Ru NPs was studied by TEM. Based on the TEM and HRTEM images shown in Fig. 2, it can be seen that loading of Ru by precipitation method and milling method leads to the formation of highly dispersed Ru NPs on the surface of Nd_2O_3 support. The Ru NPs were uniformly dispersed on the surface of the support, which is similar with that of the pristine RuO_2 NPs precursor (Fig. S1).

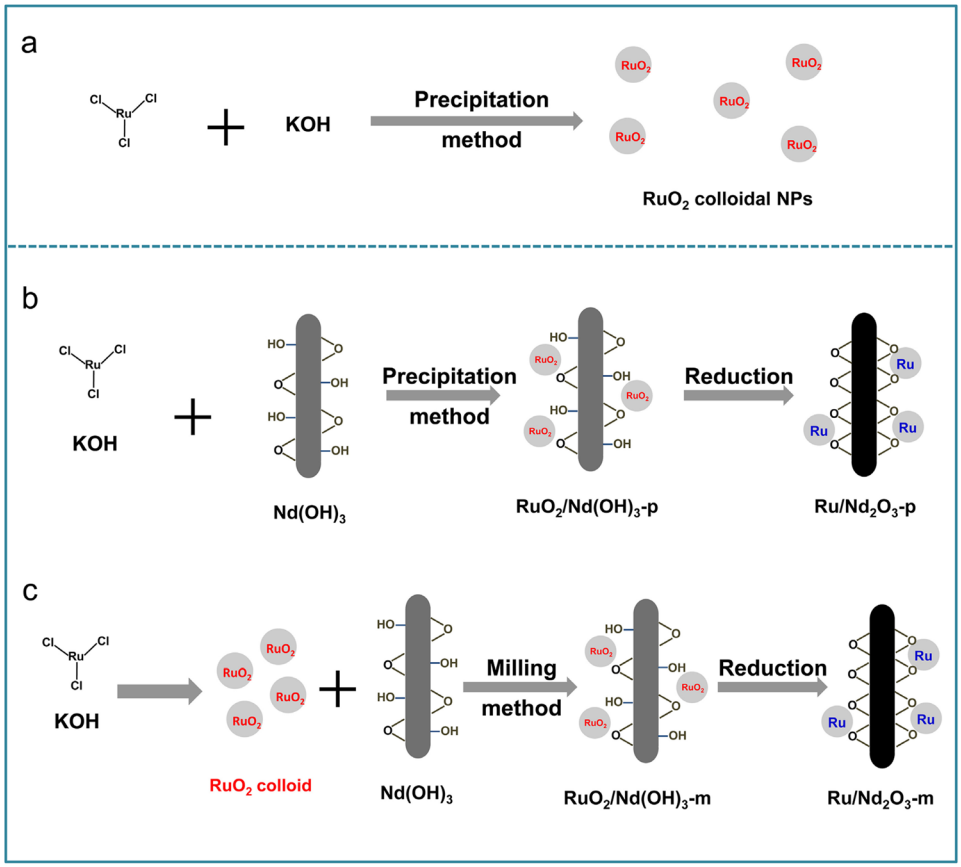

Scheme 1 Schematic illustration of formation of RuO_2 NPs (**a**) and deposition of highly dispersed Ru NPs on Nd_2O_3 support by precipitation method (**b**) and solid milling method (**c**)

Based on the Ru NPs in the images of different Ru/Nd_2O_3 samples, the average particle sizes of the Ru NPs can be preliminary estimated. The average particle sizes of the Ru NPs for the 3% Ru/Nd_2O_3-m and 3% Ru/Nd_2O_3-p from statistical analysis are about 2.6 and 2.5 nm, respectively. Meanwhile, the average particle size of Ru NPs in 1.5% Ru/ZrO_2-m and 1.5% Ru/ZrO_2-p are 2.3 and 2.4 nm, respectively, similar with that of the 3% Ru/Nd_2O_3-m and 3% Ru/Nd_2O_3-p samples. Based on the average particle size from TEM results, the Ru dispersion values of the Ru/Nd_2O_3 samples estimated are determined to be about 41–46%. Therefore, loading of Ru on the Nd_2O_3 support by impregnation and precipitation methods show no obvious influence on the Ru dispersion in Ru/Nd_2O_3-m and Ru/Nd_2O_3-p catalysts. The metal dispersion and average Ru particle size on Ru/Nd_2O_3 catalysts were also estimated from the CO chemisorption and the corresponding results are listed in Table S1. The metal dispersion for the 1.5% Ru/Nd_2O_3-p and 3% Ru/Nd_2O_3-p catalyst reaches 39.5% and 44.8%. The size of the Ru NPs from CO chemisorption is about 3.3 and 3.0 nm for the 1.5% Ru/Nd_2O_3-p and 3% Ru/Nd_2O_3-p samples, which shows a good agreement with the TEM images. Therefore, the Ru NPs in Ru/Nd_2O_3-p samples show similar particle size with that of the Ru/Nd_2O_3-m samples with similar Ru contents.

XPS analyses were performed to investigate the chemical state of the Ru NPs in different Ru/Nd_2O_3 catalysts (Fig. 3). Due to the overlapped of Ru $3d_{3/2}$ and C 1s peak at c.a. 284.8 eV, Ru state was analyzed by the peak of Ru $3d_{5/2}$ peaks. The Ru $3d_{5/2}$ peak of 1.5% Ru/Nd_2O_3-m and 3% Ru/Nd_2O_3-m was found to be about 280.1 and 280.3 eV, consistent with the Ru $3d_{5/2}$ peak observed for the metallic Ru and highly dispersed Ru metal NPs on the oxide supports (279.6–280.2 eV) [37], indicating the dominant metallic state of Ru NPs in the Ru/Nd_2O_3-m samples. Similar with Ru/Nd_2O_3-m samples, Ru $3d_{5/2}$ peak centered at 280.0 eV can also be observed in the XPS spectra of 1.5% Ru/Nd_2O_3-p and 3% Ru/Nd_2O_3-p samples, demonstrating that the similar chemical state of metallic Ru NPs in the two Ru/Nd_2O_3-p samples. Besides the peak associated with the metallic Ru species at 280.0 eV, a broad peak at about 280.9 eV can also be observed for the 1.5% Ru/Nd_2O_3-p and 3% Ru/Nd_2O_3-p samples. As the Ru NPs in all the samples have been fully reduced, the much different binding energy value of Ru $3d_{5/2}$ peak at about 280.2 and 280.9 eV can be attributed to the metallic Ru species in different electronic environment states. In particular, the Ru $3d_{5/2}$ peak at about 280.9 eV may be associated with the $Ru^{\delta+}$ species located at the interface between the Ru NPs and Nd_2O_3 support. This result demonstrates that the electronic environment of Ru NPs in the

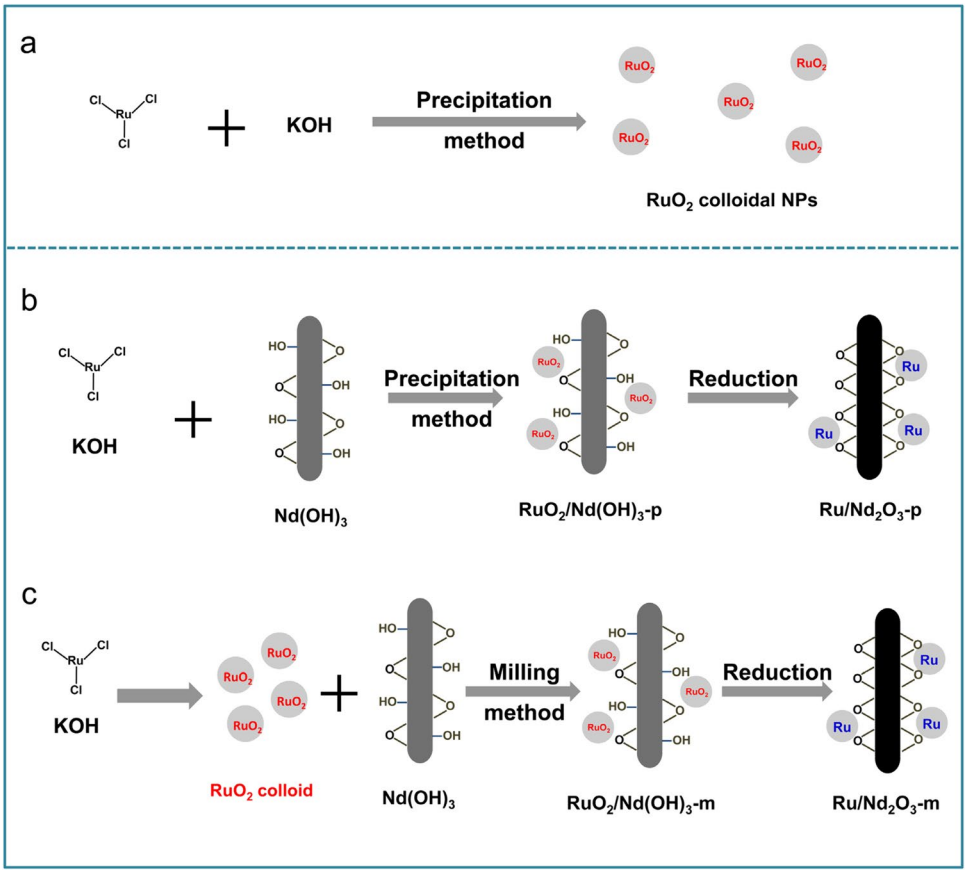

Fig. 1 XRD patterns of Nd_2O_3, 1.5% Ru/Nd_2O_3-m, 3% Ru/Nd_2O_3-m, 1.5% Ru/Nd_2O_3-p and 3% Ru/Nd_2O_3-p obtained after reaction. Standard pattern of Ru and Nd_2O_3 were included as references

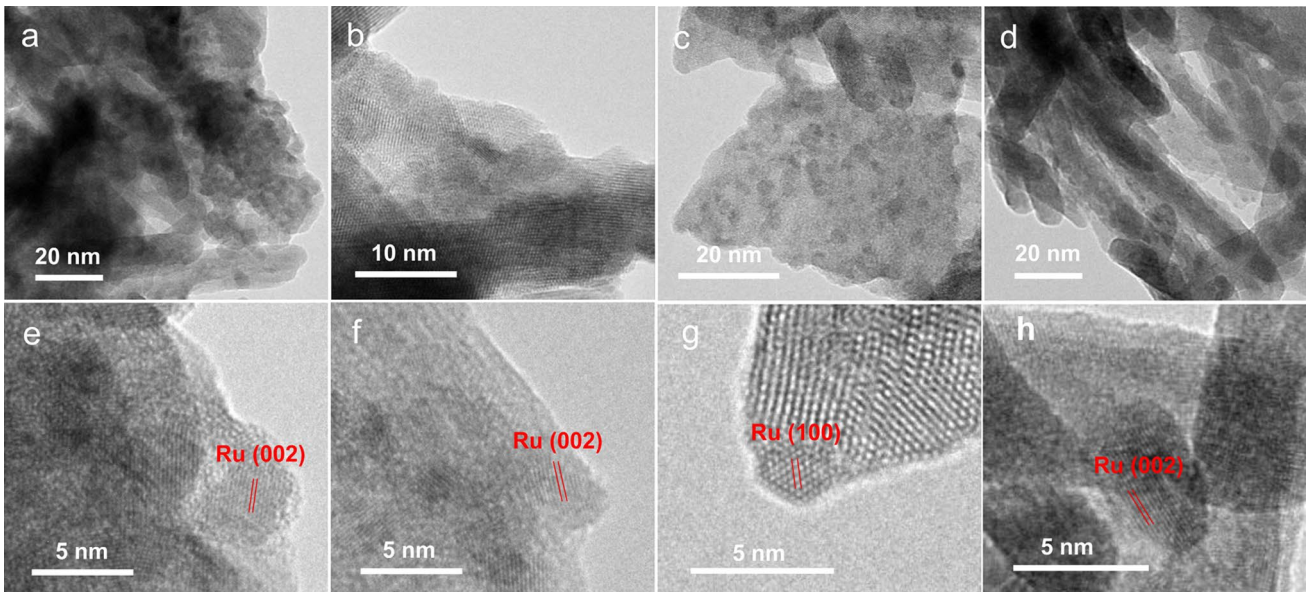

Fig. 2 TEM and HRTEM images of 1.5% Ru/Nd_2O_3-m (**a** and **e**), 3% Ru/Nd_2O_3-m (**b** and **f**), 1.5% Ru/Nd_2O_3-p (**c** and **g**) and 3% Ru/Nd_2O_3-p (**d** and **h**) obtained after reaction

Ru/Nd_2O_3-p samples is much different from that of the Ru NPs in the Ru/Nd_2O_3-m samples. Based on the Ru 3d XPS spectra (Fig. 3), the concentration of $Ru^{\delta+}$ species in total surface Ru species on the 1.5% Ru/Nd_2O_3-p sample is estimated to be about 45.0%. Compared to the 1.5% Ru/Nd_2O_3-p, 3% Ru/Nd_2O_3-p shows a relatively higher surface $Ru^{\delta+}$

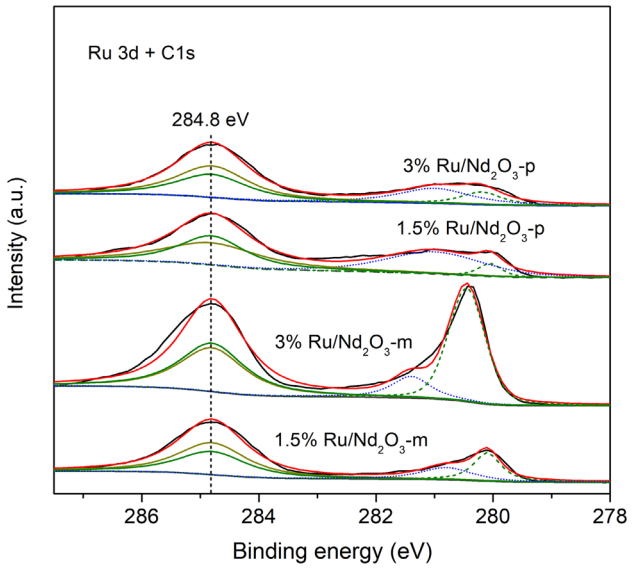

Fig. 3 Ru 3d core level XPS spectra of 1.5% Ru/Nd_2O_3-m, 3% Ru/Nd_2O_3-m, 1.5% Ru/Nd_2O_3-p and 3% Ru/Nd_2O_3-p catalysts obtained after reaction

fraction of 67.6%. TEM results reveal that nearly identical reduced Ru NPs can be observed in the different samples. An obvious XPS peak at 531.6 eV, associated with surface –OH or oxygen vacancies, can be observed in the O 1s XPS spectra of 1.5% Ru/Nd_2O_3-m, 3% Ru/Nd_2O_3-m, 1.5% Ru/Nd_2O_3-p and 3% Ru/Nd_2O_3-p catalysts samples (Fig. S2), indicating the presence of high amount of surface oxygen vacancies. At the same time, nearly identical Nd 3d XPS spectra can be observed for the different Ru/Nd_2O_3 samples (Fig. S3). However, substantial difference of chemical structure can be observed over the two samples even with nearly identical metallic Ru NPs. Considering the similar Ru NPs on the Nd_2O_3 support in different 1.5% Ru/Nd_2O_3 samples, the appearance of peak at about 280.9 eV is supposed to be caused by the presence of $Ru^{\delta+}$ species located at the interface between Ru NPs and Nd_2O_3 support, which may be beneficial for the catalytic performances in NH_3 decomposition.

3.2 Catalytic Performances of Ru/Nd_2O_3 Catalysts

Figure 4a shows the temperature dependence of NH_3 conversion obtained over Ru/Nd_2O_3 catalysts prepared by precipitation and milling method. The Ru NPs alone show very poor catalytic performance under reaction conditions (Fig. S4). However, upon dispersing Ru NPs on the Nd_2O_3 support, the catalytic performance of Ru NPs can be greatly improved (Fig. 4a). It can be seen that the catalytic activity of the catalyst Ru loaded on the same Nd_2O_3 support were greatly influenced by the preparation method. Under identical

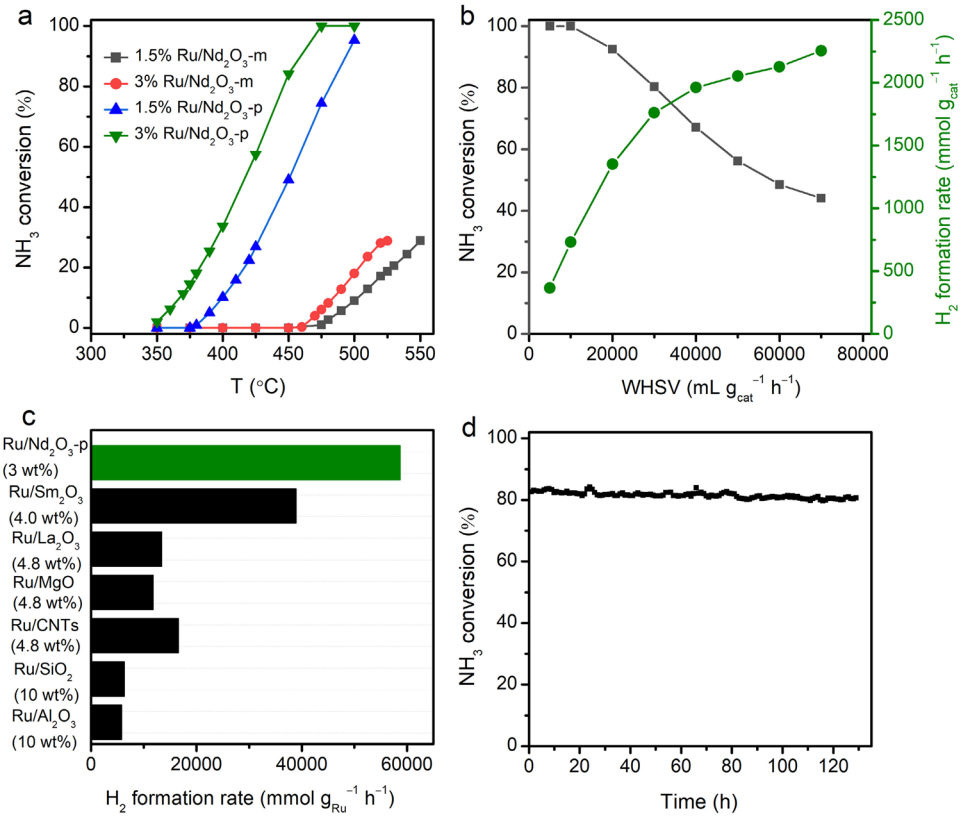

Fig. 4 **a** NH_3 conversion over 1.5% Ru/Nd_2O_3-m, 3% Ru/Nd_2O_3-m, 1.5% Ru/Nd_2O_3-p and 3% Ru/Nd_2O_3-p catalysts as a function of reaction temperature. **b** Effect of WHSV on the NH_3 conversion and H_2 formation rate of 3% Ru/Nd_2O_3-p catalyst for NH_3 decomposition at 450 °C. **c** H_2 formation rates of 3% Ru/Nd_2O_3-p and typical efficient Ru-based NH_3 decomposition catalysts at 450 °C with a WHSV of 30,000 mL g_{cat}^{-1} h^{-1}. **d** Stability test of 3% Ru/Nd_2O_3-p catalyst for NH_3 decomposition at 450 °C

conditions, the Ru/Nd_2O_3-p samples exhibit much higher catalytic activity than the Ru/Nd_2O_3-m at temperature ranging from 350 to 550 °C, implying the critical role of preparation method for the formation of efficient catalysts. The Ru/Nd_2O_3-p readily show apparent activity from 350 °C, while Ru/Nd_2O_3-m samples display negligible activity at temperature ranging from 350 to 450 °C. At the same temperature, the activities follow the order of 3% Ru/Nd_2O_3-p > 1.5% Ru/Nd_2O_3-p > 3% Ru/Nd_2O_3-m > 1.5% Ru/Nd_2O_3-m. For example, the NH_3 conversion of 3% Ru/Nd_2O_3-p can reach 84.2% at 450 °C, which is much higher than that of the 1.5% Ru/Nd_2O_3-p (49.0%). By contrast, no obvious activity can be observed over the 3% Ru/Nd_2O_3-m and 1.5% Ru/Nd_2O_3-m samples at the temperature of 450 °C.

Additionally, the catalytic performance of 3% Ru/Nd_2O_3-p was further examined with a supply of pure NH_3 at various WHSV values (5000–70,000 mL g_{cat}^{-1} h^{-1}). Figure 4b depicts effect of WHSV on the catalytic performance of 3% Ru/Nd_2O_3-p catalyst at 450 °C. It can be inferred that the higher NH_3 conversion rate directly contributes to a higher H_2 formation rate due to the absence of side reactions in NH_3 decomposition reaction. It can be seen that NH_3 conversion at 450 °C increases remarkably with decrease of WHSV because of the increase in the residence time of the reactant. At the temperature of 450 °C, nearly complete conversion (96.8%) can be obtained with a WHSV as high as 10,000 mL g_{cat}^{-1} h^{-1}. The H_2 formation rate of catalyst based on the weight of the 3% Ru/Nd_2O_3-p catalyst was calculated at various WHSV values. With the WHSV value increases from 5000 to 70,000 mL g_{cat}^{-1} h^{-1}, the H_2 formation rate of 3% Ru/Nd_2O_3-p catalyst shows a remarkable increase from 365.5 to 2250.0 mmol g_{cat}^{-1} h^{-1} at 450 °C. A comparison of activity of Ru/Nd_2O_3-p catalysts with those of the other efficient Ru-based catalysts for NH_3 decomposition reported in literatures are shown in Fig. 4c and Table 1. Under similar reaction conditions, not only the NH_3 conversion but also the H_2 formation rate of 3% Ru/Nd_2O_3-p is comparable with many of the efficient supported Ru catalysts in literatures. The H_2 formation rate of 1.5% Ru/Nd_2O_3-p and 3% Ru/Nd_2O_3-p catalyst per gram Ru is up to 859.9 and 1002.1 mmol g_{Ru}^{-1} min^{-1} at 450 °C, which is about 1.7 and 2.0 times higher than one of typical efficient Ru/MgO-DP catalyst (495.2 mmol g_{Ru}^{-1} min^{-1}) reported previously.

Above results clearly show that Nd_2O_3 is a good support for preparation of efficient supported Ru NPs-based catalysts. Apart from catalytic activity, stability is another crucial parameter for evaluation the catalytic performance of Ru/Nd_2O_3-p catalyst in NH_3 decomposition reaction. Here, a stability test of the 3% Ru/Nd_2O_3-p catalyst was also carried out at 450 °C with a relatively high WHSV of 30,000 mL g_{cat}^{-1} h^{-1}. As shown in Fig. 4d, no obvious activity loss is observed and approximately 81.0% NH_3 conversion is maintained over 120 h, demonstrating the excellent stability of 3% Ru/Nd_2O_3-p catalyst for NH_3

Table 1 NH_3 conversion and H_2 formation rate of typical supported Ru catalysts at 450 °C

Catalyst	WHSV (mL g_{cat}^{-1} h^{-1})	Ru loading (wt%)	NH_3 conversion (%)	H_2 formation rate (mmol g_{cat}^{-1} h^{-1})	H_2 formation rate (mmol g_{Ru}^{-1} min^{-1})	References
Ru/Al_2O_3	30,000	10.0	31.5	579.8	96.6	[6]
Ru/SiO_2	30,000	10.0	34.5	635.0	105.8	[6]
Ru/CNTs	30,000	4.8	43.3	796.9	276.7	[38]
Ru/MgO	30,000	4.8	30.8	566.9	196.8	[38]
Ru/TiO_2	30,000	4.8	27.2	500.6	173.8	[38]
Ru/Al_2O_3	30,000	4.8	23.3	428.8	148.9	[38]
Ru/AC	30,000	4.8	28.7	528.2	183.4	[38]
Ru/MgO	30,000	2.8	41.3	760.1	452.5	[18]
Ru/MgO	30,000	3.5	56.5	1039.9	495.2	[19]
Ru/Pr_6O_{11}	3000	5.0	100	184.0	613.5	[39]
Ru/La_2O_3	18,000	4.8	58.2	642.7	223.1	[23]
Ru/Sm_2O_3	30,000	4.0	84.6	1557.0	648.8	[27]
Ru/Y_2O_3	30,000	5.0	83.7	1540.5	513.5	[25]
Ru/Pr_2O_3	30,000	4.8	68.2	1255.2	435.8	[26]
Ru/$CaAlO_x$-w	30,000	3.5	20.0	368.1	175.3	[40]
Ru/BHA	30,000	2.7	42.0	773.0	477.2	[41]
Ru/c−MgO	30,000	4.7	80.6	1483.4	526.0	[42]
Ru/Rb−Y	30,000	2.0	24.0	441.7	375.6	[43]
Ru/Nd_2O_3-p	30,000	1.5	49.0	901.8	1002.1	This work
Ru/Nd_2O_3-p	30,000	3.0	84.1	1547.9	859.9	This work

decomposition reaction. XRD (Fig. S5) pattern of 3% Ru/Nd_2O_3-p obtained after the stability test shows that no characteristic XRD peaks associated with Ru metal phase can be observed, evidencing that no serious aggregation of Ru NPs occurred under harsh reduction conditions. TEM image (Fig. S6) further shows that the Ru NPs after 100 h reaction were uniformly distributed on the Nd_2O_3 support. The Ru NPs on the Nd_2O_3 support is the active component for NH_3 decomposition reaction. Here, the well preservation of highly dispersed Ru NPs of 3% Ru/Nd_2O_3-p at 450 °C agrees well with its high stability under NH_3 decomposition reaction conditions. Overall, the 3% Ru/Nd_2O_3-p catalyst not only gives high activity but also gives high stability, demonstrating the promise for potential application as efficient catalysts in NH_3 decomposition reaction.

3.3 Structure–Performance Relationship of Ru/Nd_2O_3-m and Ru/Nd_2O_3-p Catalysts

To clarify the origin of high activity of 4% Ru/Sm_2O_3−p, the apparent activation energy (Ea) of different Ru/Nd_2O_3-m and Ru/Nd_2O_3-p catalysts was calculated based on NH_3 conversion values far away from the equilibrium value (less than 20%). From Arrhenius-type plots (Fig. 5), it can be seen that no obvious difference in the Ea can be observed for the different Ru/Nd_2O_3-m and Ru/Nd_2O_3-p samples. The apparent activation energy of 3% Ru/Nd_2O_3-p is 142 kJ mol^{-1}, which is little smaller than that of 3% Ru/Nd_2O_3-m (132 kJ mol^{-1}). At the same time, similar Ea value can be obverted over the 1.5% Ru/Nd_2O_3-p (151 kJ mol^{-1}) and 1.5% Ru/Nd_2O_3-m (152 kJ mol^{-1}) samples. For the Ru/Nd_2O_3-m and Ru/Nd_2O_3-p samples with different Ru contents, it can be seen that the Ea values of both samples show a little decrease with increase of Ru content. Among the different Ru/Nd_2O_3 samples, the 3% Ru/Nd_2O_3-m sample gives a relatively small Ea of 132 kJ mol^{-1}.

Comparison the intrinsic activity of Ru NPs is useful for understanding the remarkable different activity of Ru/Nd_2O_3-m and Ru/Nd_2O_3-p catalysts. Usually, the H_2 formation turnover frequency (TOF_{H2}), which can be calculated by normalizing the observed H_2 formation rate (mole formed, H_2 g_{cat}^{-1} s^{-1}) to the number of exposed Ru surface atoms per gram of catalyst, is a standard parameter for the evaluation of intrinsic catalytic performance of different catalysts. Here, the TOF_{H2} of the Ru/Nd_2O_3-m and Ru/Nd_2O_3-p samples can be calculated by assuming that all surface Ru atoms act as active sites (Fig. S7). Correlating well with the catalytic activity results, a remarkable difference in the TOF_{H2} can be observed for Ru/Nd_2O_3-p catalysts in comparison with that of the Ru/Nd_2O_3-m catalysts under identical conditions. From the Fig. 5b and Fig. S2, it can be seen that the reaction rate of Ru/Nd_2O_3-p samples were significantly higher than that of Ru/Nd_2O_3-m samples for the decomposition of NH_3

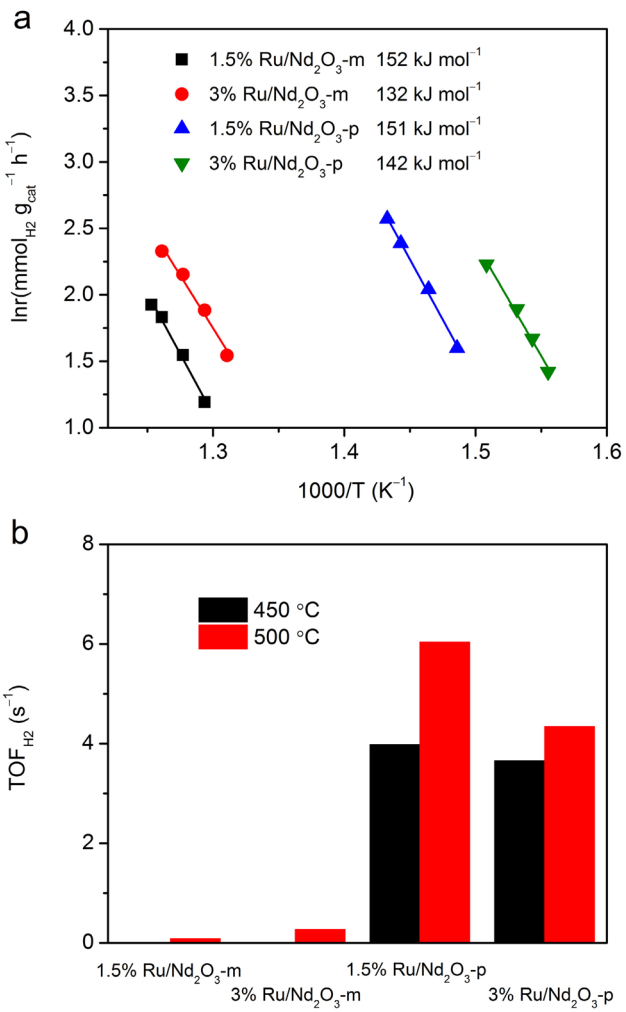

Fig. 5 **a** Arrhenius plots of 1.5% Ru/Nd_2O_3-m, 3% Ru/Nd_2O_3-m, 1.5% Ru/Nd_2O_3-p and 3% Ru/Nd_2O_3-p catalysts. **b** TOF_{H2} values of 1.5% Ru/Nd_2O_3-m, 3% Ru/Nd_2O_3-m, 1.5% Ru/Nd_2O_3-p and 3% Ru/Nd_2O_3-p at 400 and 450 °C respectively

and formation of H_2, revealing the excellent intrinsic activity of Ru NPs in Ru/Nd_2O_3-p samples. As shown in Fig. 5b, the 1.5% Ru/Nd_2O_3-p sample possesses a TOF_{H2} value of 6.04 s^{-1} at 500 °C, higher than that of the 3% Ru/Nd_2O_3-p (4.34 s^{-1}) sample. The TOF_{NH3} value of 1.5% Ru/Nd_2O_3-p at 500 °C is 67.1 and 22.4 times higher than that of the 1.5% Ru/Nd_2O_3-m (0.09 s^{-1}) and 3% Ru/Nd_2O_3-m (0.27 s^{-1}) samples. Remarkably, the TOF_{H2} value of 3% Ru/Nd_2O_3-p (4.34 s^{-1}) at 500 °C is 48.2 and 16.1 times higher than that of the 1.5% Ru/Nd_2O_3-m (0.09 s^{-1}) and 3% Ru/Nd_2O_3-m (0.27 s^{-1}) samples at the same temperature.

Metal–support interaction is widely present in oxide supported metal catalysts, and plays critical role in regulating the activity of catalysts. Here, TPR was performed to probe the metal−support interaction of the Ru/Sm_2O_3 catalysts obtained from different methods. As shown in Fig. 6, two broad peaks centered at around 127 and 213 °C,

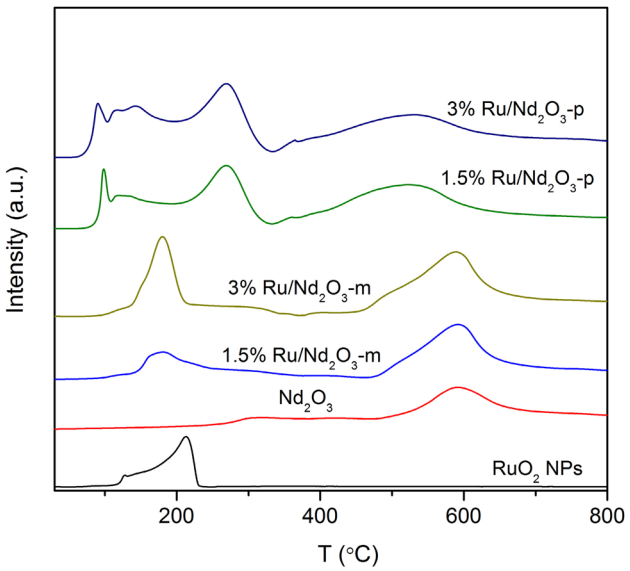

Fig. 6 TPR profiles of RuO_2 colloid, Nd_2O_3, 1.5% Ru/Nd_2O_3-m, 3% Ru/Nd_2O_3-m, 1.5% Ru/Nd_2O_3-p and 3% Ru/Nd_2O_3-p

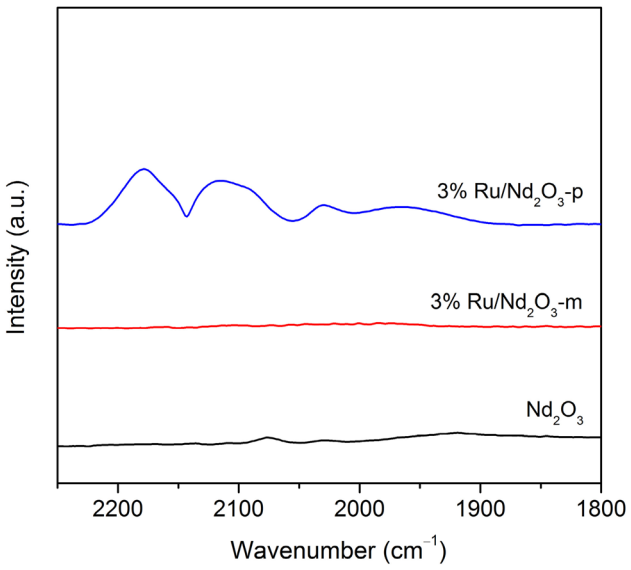

Fig. 7 DRIFTS spectra of CO adsorption on Nd_2O_3, 3% Ru/Nd_2O_3-m and 3% Ru/Nd_2O_3-p

corresponding to a two-step reduction process from RuO_2 NPs to metallic Ru NPs, can be observed in the TPR profile of RuO_2 NPs. For the 1.5% Ru/Nd_2O_3-m and 3% Ru/Nd_2O_3-m samples, two major broad reduction peaks centered at around 190 and 590 °C can be observed in the TPR profiles. The onset reduction temperature of 1.5% Ru/Nd_2O_3-m and 3% Ru/Nd_2O_3-m samples is also at about 100 °C, similar with that of the RuO_2 NPs. About three broad peaks at ca. 187 °C can be observed for 1.5% Ru/Nd_2O_3-m and 3% Ru/Nd_2O_3-m samples. In combination with the TPR profile of Nd_2O_3, we can reasonably ascribe the reduction peaks at temperature below 240 °C to the reduction of the RuO_2 NPs in Ru/Nd_2O_3−m samples while reduction peaks at temperature above 240 °C can be attributed to reduction of surface oxygen on Nd_2O_3 support. As shown in Fig. 6, major part of RuO_2 NPs in Ru/Nd_2O_3−m samples can be reduced at temperature below 180 °C, similar with free standing RuO_2 and Ru/Nd_2O_3-m samples. For the 1.5% Ru/Nd_2O_3-p and 3% Ru/Nd_2O_3-p sample, four broad peaks centered at 90, 120, 240 and 510 °C can be observed in the TPR profiles. The onset reduction temperature of 1.5% Ru/Nd_2O_3-p and 3% Ru/Nd_2O_3-p sample is about 53 °C, along with three reduction peaks centered at 84, 104, 122 and 240 °C, respectively. In comparison with that of the RuO_2 NPs in Ru/Nd_2O_3-m sample, RuO_2 NPs in Ru/Nd_2O_3-p samples give much different reduction behavior. Both the onset and peak reduction temperature of the Ru/Nd_2O_3-p catalysts shift towards low temperature, revealing the enhanced interaction between the RuO_2 NPs and Nd_2O_3. Consider the similar and uniform dispersion of Ru NPs in different Ru/Nd_2O_3 samples, the difference of reduction peaks indicates that much enhanced interaction between RuO_2 NPs and Nd_2O_3 support in Ru/Nd_2O_3-p samples. The enhanced interaction between the RuO_2 NPs and Nd_2O_3 can not only facilitate the reduction of RuO_2 NPs but also promote the reduction of surface oxygen of the Nd_2O_3 support. At the same time, the reduction peaks associated with the reduction of surface oxygen of the Nd_2O_3 support show an obvious decrease towards lower temperature.

DRIFTS of CO adsorption spectroscopy was applied to investigate the metal–support interaction of different catalysts. The DRIFTS spectra of adsorbed CO on the different catalysts, including 3% Ru/Nd_2O_3-m and 3% Ru/Nd_2O_3-p samples, are presented in Fig. 7. The 3% Ru/Nd_2O_3-p sample displays four bands, i.e., 2180, 2115 cm^{-1}, 2039–2062 cm^{-1} and 1900–2025 cm^{-1}, similar to those reported in previous literatures. Generally, the CO bands originated from CO adsorption on supported Ru catalysts can be divided into three kinds of groups: high frequency 1 (HF1) at 2156–2133 cm^{-1}, high frequency 2 (HF2) at 2100–2060 cm^{-1} and low frequency (LF) at 2060–1970 cm^{-1}. According to the literature results, the HF2 and LF bands at 2039 and 1965 cm^{-1} are ascribed to the linearly adsorbed CO and bridge bonded CO on the low-coordinated surface Ru atoms located on metallic Ru NPs [44–47], while the HF1 band at 2180 and 2115 cm^{-1} is usually assigned to the multi-carbonyl species on the partially oxidized Ru sites [$Ru^{\delta+}(CO)_x$] on the oxide supports [48, 49]. The CO bands originated from CO adsorption on supported Ru NPs in Ru/Nd_2O_3 samples were significantly influenced by the preparation method. Different from that of the 3% Ru/Nd_2O_3-p sample, the CO DRIFTS spectra

of 3% Ru/Nd_2O_3-m does not show any adsorption band in the wide region, which should have direct relation with the metal–support interaction in Ru/Nd_2O_3 catalysts. As the partially oxidized Ru sites [$Ru^{\delta+}(CO)_x$] are usually located at the interface of Ru NPs–oxide support, we can reasonably conclude that the interaction between Ru NPs and oxide support can be enhanced in 3% Ru/Nd_2O_3-p samples.

NH_3 decomposition reaction over Ru-based catalysts is known to be a structure–sensitive reaction. Due to the change of concentration of active B5 sites on the surface of Ru NPs, the size of Ru NPs play crucial role in tuning the catalytic performances of the Ru-based catalysts [50–52]. It worthy of mentioning that NH_3 synthesis, a rise in TOF over promoted Ru/Al_2O_3 and AC-supported Ru catalysts has been observed with increase of size of Ru particles [50, 51]. It has been found that NH_3 decomposition on supported Ru catalysts is also highly structure sensitive, with TOF_{H2} values increasing by almost 2 orders of magnitude as the particle size increases from 0.8 to > 7 nm [52]. Here, the different Ru/Nd_2O_3 catalysts were obtained from the same $Nd(OH)_3$ support precursor and RuO_2 colloid NPs. At the same time, TEM images and CO chemisorption results show that Ru NPs were distributed uniformly on the Nd_2O_3 support with similar particle size in different Ru/Nd_2O_3 samples. However, it could be seen that the H_2 formation rate and TOF_{NH3} value of Ru/Nd_2O_3-p samples were significantly higher than that of Ru/Nd_2O_3-m samples with similar Ru NPs under identical conditions. Thus, the particle size of Ru NPs may not be the key factor in causing the difference of the catalytic performances of Ru/Nd_2O_3-m and Ru/Nd_2O_3-p catalysts studied here. The remarkable increase in the catalytic activity and intrinsic activity of Ru/Nd_2O_3-p catalysts should be highly related with other important key structure factor rather than particle size of Ru NPs.

For oxide supported Ru NPs catalysts, structural factors such as the dispersion, size and morphology of Ru NPs, interaction between Ru NPs and support, and surface property of support can influence the surface structure and chemical state of Ru NPs, leading to a great difference in the catalytic activity. Based on the similar particle size and metal dispersion of Ru NPs and similar composition in the different Ru/Nd_2O_3 samples, we propose that the remarkable difference of intrinsic activity in Ru/Nd_2O_3-m and Ru/Nd_2O_3-p catalysts may arise from the difference in the metal–oxide interaction in different catalysts. In combination with the TEM, XPS, TPR and CO DRIFTS results, we can correlate the observed remarkable different activity of Ru/Nd_2O_3 catalyst to the difference of metal–support interaction. TEM results reveal that similar Ru NPs can be observed in the different samples. However, substantial difference of chemical structure can be observed over the two samples even with similar Ru NPs. For the Ru/Nd_2O_3-p with relatively strong metal–oxide interaction, the relative high binding energy value of Ru 3d associated with the presence of $Ru^{\delta+}$ species located at the interface between Ru NPs and Nd_2O_3 support can be detected. Thus, it is worthwhile to emphasize the critical role of metal–support interaction in modulating the electronic structure and intrinsic activity of Ru NPs in different Ru/Nd_2O_3 catalysts. Suitable metal–support interaction is believed to be beneficial for improving the catalytic performance of Ru/Nd_2O_3 catalysts for NH_3 decomposition, and much enhanced TOF_{H2} can be observed even the sample has similar particle size of Ru NPs. We believe that this phenomenon is highly related to the change in the adsorption strength of the reactants and products on the similar Ru NPs in different Ru/Nd_2O_3 catalysts. It has been generally considered that the associative desorption of nitrogen atoms from the catalyst surface is the rate-determining step in NH_3 decomposition reaction. Considering that B5 site on the Ru NPs is the active site for NH_3 decomposition, above results confirm that the modulated electron structure of Ru NPs can eventually change activation and dissociation of adsorbed NH_3 on the surface of Ru/Nd_2O_3-p catalysts during NH_3 decomposition. At the same time, it can be expected that the interaction between Ru NPs and Nd_2O_3 support can change in the electronic property of the metallic Ru NPs and weaken strong adsorption of nitrogen atoms and further facilitate associative desorption of nitrogen atoms from the B5 active sites on the Ru NPs in Ru/Nd_2O_3-p catalysts. The easy desorption of dissociated nitrogen atoms from the B5 active sites on the Ru NPs made the residence time of reactants at active sites shorter and provide more active sites for the decomposition of NH_3 molecules, leading to a faster reaction rate in NH_3 decomposition reaction.

4 Conclusions

In summary, we have explored the potential of Nd_2O_3 supported Ru NPs as a new efficient catalyst for NH_3 decomposition using Ru/Nd_2O_3 prepared via precipitation and milling method. We found that the Ru/Nd_2O_3-p catalysts from precipitation method give much higher activity than that of the Ru/Nd_2O_3-m analogues from milling method with nearly identical Ru NP in NH_3 decomposition. A detailed analysis based on the XRD, TEM, XPS, TPR and CO DRIFTS characterization results reveal that enhancing metal–support interaction can modulate the electronic structure of Ru NPs and efficiently enhance the intrinsic activity of Ru NPs in the Ru/Nd_2O_3-p catalysts. In view of the excellent activity and robust stability achieved by the Ru/Nd_2O_3-p catalysts, this work offers promise to improve the catalytic performance of Ru-based catalysts by delicately modulating metal–support interaction.

Supplementary Information The online version contains supplementary material available at https://doi.org/10.1007/s11244-024-01926-8.

Acknowledgements We acknowledge the financial support from the National Key Research and Development Program of China (2022YFB4002400), the Natural Science Foundation of China (22179128), the Joint Fund of the Yulin University and the Dalian National Laboratory for Clean Energy (YLU-DNL Fund 2021010) and the Liaoning Revitalization Talents Program (XLYC2002076).

Data availability All data used during the study are available in a repository or online in accordance with funder data retention policies.

References

1. He T, Pachfule P, Wu H, Xu Q, Chen P (2016) Hydrogen carriers. Nat Rev Mater 1(12):17. https://doi.org/10.1038/natrevmats.2016.59
2. Klerke A, Christensen CH, Norskov JK, Vegge T (2008) Ammonia for hydrogen storage: challenges and opportunities. J Mater Chem 18(20):2304–2310. https://doi.org/10.1039/b720020j
3. Lan R, Irvine JTS, Tao SW (2012) Ammonia and related chemicals as potential indirect hydrogen storage materials. Int J Hydrogen Energy 37(2):1482–1494. https://doi.org/10.1016/j.ijhydene.2011.10.004
4. Metkemeijer R, Achard P (1994) Comparison of ammonia and methanol applied indirectly in a hydrogen fuel-cell. Int J Hydrogen Energy 19(6):535–542. https://doi.org/10.1016/0360-3199(94)90009-4
5. Klerke A, Christensen CH, Nørskov JK, Vegge T (2008) Ammonia for hydrogen storage: challenges and opportunities. J Mater Chem 18(20):2304. https://doi.org/10.1039/b720020j
6. Choudhary TV, Sivadinarayana C, Goodman DW (2001) Catalytic ammonia decomposition: COx-free hydrogen production for fuel cell applications. Catal Lett 72(3–4):197–201. https://doi.org/10.1023/A:1009023825549
7. Yin SF, Xu BQ, Ng CF, Au CT (2004) Nano Ru/CNTs: a highly active and stable catalyst for the generation of COx-free hydrogen in ammonia decomposition. Appl Catal B 48(4):237–241. https://doi.org/10.1016/j.apcatb.2003.10.013
8. Yin SF, Xu BQ, Wang SJ, Ng CF, Au CT (2004) Magnesia-carbon nanotubes (MgO-CNTs) nanocomposite: novel support of Ru catalyst for the generation of COx-free hydrogen from ammonia. Catal Lett 96(3–4):113–116. https://doi.org/10.1023/B:Catl.0000030107.64702.74
9. Ganley JC, Thomas FS, Seebauer EG, Masel RI (2004) A priori catalytic activity correlations: the difficult case of hydrogen production from ammonia. Catal Lett 96(3–4):117–122. https://doi.org/10.1023/B:Catl.0000030108.50691.D4
10. Hill AK, Torrente-Murciano L (2015) Low temperature H-2 production from ammonia using ruthenium-based catalysts: synergetic effect of promoter and support. Appl Catal B 172:129–135. https://doi.org/10.1016/j.apcatb.2015.02.011
11. Yin SF, Zhang QH, Xu BQ, Zhu WX, Ng CF, Au CT (2004) Investigation on the catalysis of COx-free hydrogen generation from ammonia. J Catal 224(2):384–396. https://doi.org/10.1016/j.jcat.2004.03.008
12. Mukherjee S, Devaguptapu SV, Sviripa A, Lund CRF, Wu G (2018) Low-temperature ammonia decomposition catalysts for hydrogen generation. Appl Catal B 226:162–181. https://doi.org/10.1016/j.apcatb.2017.12.039
13. Li YX, Yao LH, Song YY, Liu SQ, Zhao J, Ji WJ, Au CT (2010) Core-shell structured microcapsular-like Ru@SiO2 reactor for efficient generation of COx-free hydrogen through ammonia decomposition. Chem Commun 46(29):5298–5300. https://doi.org/10.1039/c0cc00430h
14. Li XK, Ji WJ, Zhao J, Wang SJ, Au CT (2005) Ammonia decomposition over Ru and Ni catalysts supported on fumed SiO_2, MCM-41, and SBA-15. J Catal 236(2):181–189. https://doi.org/10.1016/j.jcat.2005.09.030
15. Li G, Kanezashi M, Tsuru T (2011) Highly enhanced ammonia decomposition in a bimodal catalytic membrane reactor for COx-free hydrogen production. Catal Commun 15(1):60–63. https://doi.org/10.1016/j.catcom.2011.08.011
16. Okal J, Zawadzki M, Kepinski L, Krajczyk L, Tylus W (2007) The use of hydrogen chemisorption for the determination of Ru dispersion in Ru/gamma-alumina catalysts. Appl Catal A 319:202–209. https://doi.org/10.1016/j.apcata.2006.12.005
17. Larichev YV (2011) Effect of Cs+ promoter in Ru/MgO catalysts. J Phys Chem C 115(3):631–635. https://doi.org/10.1021/jp109737p
18. Zhang J, Xu HY, Ge QJ, Li WZ (2006) Highly efficient Ru/MgO catalysts for NH3 decomposition: synthesis, characterization and promoter effect. Catal Commun 7(3):148–152. https://doi.org/10.1016/j.catcom.2005.10.002
19. Ju XH, Liu L, Yu P, Guo JP, Zhang XL, He T, Wu GT, Chen P (2017) Mesoporous Ru/MgO prepared by a deposition-precipitation method as highly active catalyst for producing COX-free hydrogen from ammonia decomposition. Appl Catal B 211:167–175. https://doi.org/10.1016/j.apcatb.2017.04.043
20. Wang ZQ, Qu YM, Shen XL, Cai ZF (2019) Ruthenium catalyst supported on Ba modified ZrO2 for ammonia decomposition to COx-free hydrogen. Int J Hydrogen Energy 44(14):7300–7307. https://doi.org/10.1016/j.ijhydene.2019.01.235
21. Yin SF, Xu BQ, Wang SJ, Au CT (2006) Nanosized Ru on high-surface-area superbasic ZrO2-KOH for efficient generation of hydrogen via ammonia decomposition. Appl Catal A 301(2):202–210. https://doi.org/10.1016/j.apcata.2005.12.005
22. Zhang T, Ju XH, Liu LY, Liu L, He T, Xu YH, Wang HY, Chen P (2023) Steering ammonia decomposition over Ru nanoparticles on ZrO2 by enhancing metal-support interaction. Catal Sci Technol. https://doi.org/10.1039/d3cy00691c
23. Huang CQ, Yu YZ, Yang JM, Yan Y, Wang DS, Hu FY, Wang XW, Zhang RB, Feng G (2019) Ru/La2O3 catalyst for ammonia decomposition to hydrogen. Appl Surf Sci 476:928–936. https://doi.org/10.1016/j.apsusc.2019.01.112
24. Wang ZQ, Cai ZF, Wei Z (2019) Highly active ruthenium catalyst supported on barium hexaaluminate for ammonia decomposition to COx-free hydrogen. Acs Sustain Chem Eng 7(9):8226–8235. https://doi.org/10.1021/acssuschemeng.8b06308
25. Feng J, Liu L, Ju XH, Wang JM, Zhang XL, He T, Chen P (2021) Highly dispersed ruthenium nanoparticles on Y2O3 as superior catalyst for ammonia decomposition. ChemCatChem 13(6):1552–1558. https://doi.org/10.1002/cctc.202001930
26. Zhang XL, Liu L, Feng J, Ju XH, Wang JM, He T, Chen P (2022) Ru nanoparticles on Pr2O3 as an efficient catalyst for hydrogen production from ammonia decomposition. Catal Lett 152(4):1170–1181. https://doi.org/10.1007/s10562-021-03709-2
27. Zhang XL, Liu L, Feng J, Ju XH, Wang JM, He T, Chen P (2021) Metal-support interaction-modulated catalytic activity of Ru nanoparticles on Sm2O3 for efficient ammonia decomposition. Catal Sci Technol 11(8):2915–2923. https://doi.org/10.1039/d1cy00080b
28. Xu H, Cai HH, Luo ZK, Ren XZ, Liu JH, Chen P, Zhao FQ, Tian DY (2003) Synthesis and combustion catalysis of nanometer-sized neodymium oxide. Chin J Inorg Chem 19(6):627–630
29. Rosid SJM, Toemen S, Abu Bakar WAW, Zamani AH, Mokhtar W (2019) Physicochemical characteristic of neodymium oxide-based catalyst for in-situ CO2/H(2)methanation reaction. J Saudi Chem Soc 23(3):284–293. https://doi.org/10.1016/j.jscs.2018.08.002

30. Narasimharao K, Ali TT (2020) leInfluence of synthesis conditions on physico-chemical and photocatalytic properties of rare earth (Ho, Nd and Sm) oxides. J Mater Res Technol Jmr&T 9(2):1819–1830. https://doi.org/10.1016/j.jmrrt.2019:12.014
31. Ronduda H, Zybert M, Dziewulska A, Patkowski W, Sobczak K, Ostrowski A, Rarog-Pilecka W (2023) Ammonia synthesis using Co catalysts supported on MgO-Nd2O3 mixed oxide systems: effect of support composition. Surf Interfaces. https://doi.org/10.1016/j.surfin.2022.102530
32. Patkowski W, Zybert M, Ronduda H, Gawronska G, Albrecht A, Moszynski D, Fidler A, Dluzewski P, Rarog-Pilecka W (2023) The influence of active phase content on properties and activity of Nd2O3-supported cobalt catalysts for ammonia synthesis. Catalysts. https://doi.org/10.3390/catal13020405
33. van Deelen TW, Hernández Mejía C, de Jong KP (2019) Control of metal-support interactions in heterogeneous catalysts to enhance activity and selectivity. Nat Catal 2(11):955–970. https://doi.org/10.1038/s41929-019-0364-x
34. Lou Y, Xu J, Zhang Y, Pan C, Dong Y, Zhu Y (2020) Metal-support interaction for heterogeneous catalysis: from nanoparticles to single atoms. Mater Today Nano. https://doi.org/10.1016/j.mtnano.2020.100093
35. Wang X, Li Y (2002) Synthesis and characterization of lanthanide hydroxide single-crystal nanowires. Angew Chem Int Ed 41(24):4790–4793. https://doi.org/10.1002/anie.200290049
36. Borodziński A, Bonarowska M (1997) Relation between crystallite size and dispersion on supported metal catalysts. Langmuir 13(21):5613–5620. https://doi.org/10.1021/la962103u
37. Larichev YV (2008) Valence state study of supported ruthenium Ru/MgO catalysts. J Phys Chem C 112(38):14776–14780. https://doi.org/10.1021/jp803742g
38. Wang SJ, Yin SF, Li L, Xu BQ, Ng CF, Au CT (2004) Investigation on modification of Ru/CNTs catalyst for the generation of COx-free hydrogen from ammonia. Appl Catal B 52(4):287–299. https://doi.org/10.1016/j.apcatb.2004.05.002
39. Nagaoka K, Honda K, Ibuki M, Sato K, Takita Y (2010) Highly active Cs2O/Ru/Pr6O11 as a catalyst for ammonia decomposition. Chem Lett 39(9):918–919. https://doi.org/10.1246/cl.2010.918
40. Zhao J, Xu S, Wu H, You Z, Deng L, Qiu X (2019) Metal-support interactions on Ru/CaAlOx catalysts derived from structural reconstruction of Ca-Al layered double hydroxides for ammonia decomposition. Chem Commun (Camb) 55(96):14410–14413. https://doi.org/10.1039/c9cc05706d
41. Hu XC, Wang WW, Si R, Ma C, Jia CJ (2019) Hydrogen production via catalytic decomposition of NH3 using promoted MgO-supported ruthenium catalysts. Sci China Chem 62(12):1625–1633. https://doi.org/10.1007/s11426-019-9578-8
42. Ju X, Liu L, Zhang X, Feng J, He T, Chen P (2019) Highly efficient Ru/MgO catalyst with surface-enriched basic sites for production of hydrogen from ammonia decomposition. ChemCatChem 11(16):4161–4170. https://doi.org/10.1002/cctc.201900306
43. Cha J, Lee T, Lee Y-J, Jeong H, Jo YS, Kim Y, Nam SW, Han J, Lee KB, Yoon CW, Sohn H (2021) Highly monodisperse sub-nanometer and nanometer Ru particles confined in alkali-exchanged zeolite Y for ammonia decomposition. Appl Catal B. https://doi.org/10.1016/j.apcatb.2020.119627
44. Chin SY, Williams CT, Amiridis MD (2006) FTIR studies of CO adsorption on Al2O3- and SiO2-supported Ru catalysts. J Phys Chem B 110(2):871–882. https://doi.org/10.1021/jp053908q
45. Peden CHF, Goodman DW, Weisel MD, Hoffmann FM (1991) In situ FT-IRAS study of the co oxidation reaction over ru(001) 1. Evidence for an Eley-Rideal mechanism at high-pressures. Surf Sci 253(1–3):44–58. https://doi.org/10.1016/0039-6028(91)90580-l
46. Opre Z, Ferri D, Krumeich F, Mallat T, Baiker A (2007) Insight into the nature of active redox sites in Ru-containing hydroxyapatite by DRIFT spectroscopy. J Catal 251(1):48–58. https://doi.org/10.1016/j.jcat.2007.07.017
47. Chen H-T (2012) First-principles study of CO adsorption and oxidation on Ru-doped CeO2(111) surface. J Phys Chem C 116(10):6239–6246. https://doi.org/10.1021/jp210864m
48. Yokomizo GH, Louis C, Bell AT (1989) An infrared study of co adsorption on reduced and oxidized Ru/SiO_2. J Catal 120(1):1–14. https://doi.org/10.1016/0021-9517(89)90245-5
49. Assmann J, Narkhede V, Khodeir L, Loffler E, Hinrichsen O, Birkner A, Over H, Muhler M (2004) On the nature of the active state of supported ruthenium catalysts used for the oxidation of carbon monoxide: steady-state and transient kinetics combined with in situ infrared spectroscopy. J Phys Chem B 108(38):14634–14642. https://doi.org/10.1021/jp0401675
50. Murata S, Aika K (1992) Preparation and characterization of chlorine-free ruthenium catalysts and the promoter effect in ammonia-synthesis. 1. An alumina-supported ruthenium catalyst. J Catal 136(1):110–117. https://doi.org/10.1016/0021-9517(92)90110-4
51. Liang CH, Wei ZB, Xin Q, Li C (2001) Ammonia synthesis over Ru/C catalysts with different carbon supports promoted by barium and potassium compounds. Appl Catal A 208(1–2):193–201. https://doi.org/10.1016/s0926-860x(00)00713-4
52. Karim AM, Prasad V, Mpourmpakis G, Lonergan WW, Frenkel AI, Chen JGG, Vlachos DG (2009) Correlating particle size and shape of supported Ru/gamma-Al2O3 catalysts with NH3 decomposition activity. J Am Chem Soc 131(34):12230–12239. https://doi.org/10.1021/ja902587k